

Hydrogen insertion in Pd core/Pt shell cubo-octahedral nanoparticles

A. Lebon

Laboratoire de Magnétisme de Bretagne, EA 4522 Université de Brest, 6 avenue Victor Le Gorgeu, F-29285 Brest Cedex, France

A. García-Fuente and A. Vega

Departamento de Física Teórica, Atómica, y Óptica, Universidad de Valladolid, E-47011 Valladolid, Spain

F. Aguilera-Granja

Instituto de Física "Manuel Sandoval Vallarta," Universidad Autónoma de San Luis Potosí, San Luis Potosí 78000, México

(Received 31 August 2010; revised manuscript received 28 December 2010; published 30 March 2011)

We report a theoretical density functional theory study of the absorption and adsorption of hydrogen in Pd core/Pt shell cubo-octahedral nanoparticles of 55 and 147 atoms. We have explored all the possible sites available for hydrogen loading. The relative stability of H in the different sites is calculated and discussed in terms of the local geometrical and chemical environments. As a general trend, the most stable absorption sites are pyramidal interstices at the interface offering a volume for H around $2 \times 2.60 \text{ \AA}^3$, with a moderate atomic rearrangement upon H insertion and in which the H atom maximizes the number of Pd neighbors. Our theoretical findings give support to the recent hydrogen pressure-composition isotherms and NMR measurements carried out in this type of bimetallic nanoparticle [Kobayashi *et al.*, *J. Am. Chem. Soc.* **130**, 1818 (2008)].

DOI: [10.1103/PhysRevB.83.125427](https://doi.org/10.1103/PhysRevB.83.125427)

PACS number(s): 73.22.-f, 88.20.fn, 88.30.R-

I. INTRODUCTION

Understanding the physics of hydrogen in different environments is appealing for technological purposes, for instance, in environmentally clean fuel cell design or, in a more general context, in controlling or tuning certain properties of the host via hydrogen insertion. The bonding of hydrogen can be of different types depending on its atomic and chemical neighborhood, and therefore, a big effort is being made in the search for different kinds of host materials able to store H.

As to metal-based hosts, many materials have been studied both experimentally and theoretically, such as the alkaline-earth hydrides¹ or the borohydrides.^{2,3} They offer promising weight-storage ratios with hydrogen percentage values as high as 20.8% for the $\text{Mg}(\text{BH}_4)_2$.³ Transition metal elements can also form interesting alloys⁴ with H storage capability. Significant efforts have been devoted to finding metallic systems with particular geometrical and interfacial characteristics that exhibit interesting properties in regard to H loading. An example is the Fe/V multilayers, in which H insertion has been widely investigated from both experimental⁵⁻⁹ and theoretical^{10,11} viewpoints, motivated by the drastic changes in their electronic and structural properties upon H loading. In these multilayers, H prefers a V-rich environment, and it produces a lattice expansion accompanied by an increase of the magnetic moment in Fe. Baldi *et al.* have recently published a work on the hydrogen absorption properties of Pd-capped Mg/Ti multilayers.¹² They observe an out-of-plane expansion of Mg and Ti on hydrogenation, indicating strong plastic distortions in the system. Absorption isotherms can be interpreted as a result of the elastic clamping arising from strongly bonded Mg/Pd and broken Mg/Ti interfaces. This work illustrates an example of how distortions of the system may trigger the H absorption properties. Another recent study of interfacial systems, which is the focus of the present work, concerns hydrogen adsorption in core/shell Pd/Pt nanoparticles (NPs).

Kobayashi *et al.*¹³ have experimentally investigated Pd/Pt bimetallic NPs with Pd core/Pt shell structure. Their hydrogen pressure-composition isotherms and NMR measurements have shown that those NPs can absorb hydrogen; moreover, the loaded hydrogen lies preferentially around the interface. The same group has demonstrated more recently the possibility of transforming those core/shell particles into atomic alloy particles (with the same stoichiometry) by a process of hydrogen adsorption-desorption together with thermal energy.¹⁴ They have shown that, also for this chemical order, the hydrogen is preferentially absorbed in the space where Pd and Pt are in direct contact with each other.

Bimetallic Pd-Pt NPs are also very interesting from a fundamental viewpoint. We note that Pd bulk has high H storage ability, larger than that of Pd NPs,^{15,16} whereas the opposite is true in the case of Pt; that is, Pt bulk has a very low storage ability that increases in Pt NPs.¹⁷ Therefore, interesting behaviors are expected when combining these two elements that display opposite H absorption properties in their respective bulk and cluster limits. A clear example is provided in the experimental study of Kobayashi *et al.*¹³ for core/shell Pd/Pt NPs. In addition, these bimetallic core/shell NPs belong to a very promising family of compounds that are gaining a growing interest because of their activity as catalysts. In fact, in the process of extracting hydrogen from hydrocarbons, the reaction products contain H_2 and a significant amount of CO; the latter is eliminated in a preferential oxidation (PROX). It was recently demonstrated that *M*/Pt core/shell NPs, where *M* = Ru, Rh, Ir, and Pd, enhance the PROX reaction of CO mediated by hydrogen.¹⁸ The decomposition of H_2 into 2 H atoms and its adsorption or absorption on surface or interface sites is an intermediate reaction that enters in the mechanism of the PROX reaction. Despite their reduced Pt content these NPs afford the design of more active PROX catalysts. Other core/shell nanoparticles, like Pd/FePt,

are active and durable catalysts for the oxygen reduction reaction.¹⁹ Understanding the interaction of H with core/shell NPs appears to be a major issue to improve the properties of these catalysts. To better understand the physics at the surface and interface of this system, we have conducted calculations using the density functional theory (DFT), as implemented in the SIESTA code, for Pd core/Pt shell NPs of 55 and 147 atoms with cubo-octahedral symmetry in which we have considered H absorption in all the nonequivalent sites. We have taken the fcc cubo-octahedral structure following the experimental characterization, but structural relaxation has been performed in all cases. These two different sizes enable us to explore the region of small clusters (55 atoms) and the region of relatively large ones (147 atoms). Although the NPs grown by different experimental groups are larger than ours (diameters of between 3 and 6 nm), we note that the electronic structure of our 147-atom clusters already resembles that of larger clusters or bulk-like systems since the discrete-like spectrum typical of small finite clusters is lost, even when lowering the electronic temperature below 60 K (5 meV), as we discuss below. Going beyond this size would require a huge computational cost at the DFT level of accuracy.

We believe that the results of the present study will be of interest not only in the context of the experiments of Pd-Pt NPs but also for the scientific community investigating the hydrogen absorption in interfacial and mixed-metal systems. These systems are also very interesting in catalysis since they are used, for example, in catalytic converters in automobiles.²⁰ Thus, important efforts have been devoted so far to investigate different sizes and chemical orders of these bimetallic NPs.^{21–23}

The essential technical details of the calculations are described in Sec. II. In Sec. III we present and discuss the results in comparison to the experimental findings. In Sec. IV we summarize our main conclusions.

II. THEORY AND COMPUTATIONAL DETAILS

Our calculations have been performed using the DFT code SIESTA.^{24–26} The nonlocal exchange and correlation potential parametrized by Perdew, Burke, and Ernzerhof²⁷ has been chosen for the calculations. We replaced the atomic core by a nonlocal norm-conserving Troullier-Martins pseudopotential,²⁸ which was factorized in the Kleinman-Bylander form.²⁹ The ionic pseudopotentials were generated using the following atomic configurations: $4d^9, 5s^1$, and $5p^0$ for Pd and $5d^9, 6s^1$, and $6p^0$ for Pt. Cutoff radii are reported elsewhere.³⁰ We have included nonlinear core corrections.³¹ The pseudopotential of H is trivial. Within the same DFT approximation, these pseudopotentials have been tested through the comparison of the eigenvalues of different electronic configurations of the respective isolated atoms against the corresponding all electron eigenvalues. Concerning the basis sets, we have described the valence states using double- ζ -polarized³² pseudoatomic orbitals for Pd, Pt, and H.

A 200-Ry energy cutoff is used to integrate in real space. We also smoothed the Fermi distribution with an electronic temperature.²⁴ For its default value of 300 K, a very smooth spectrum for our 147-atom clusters instead of the discrete

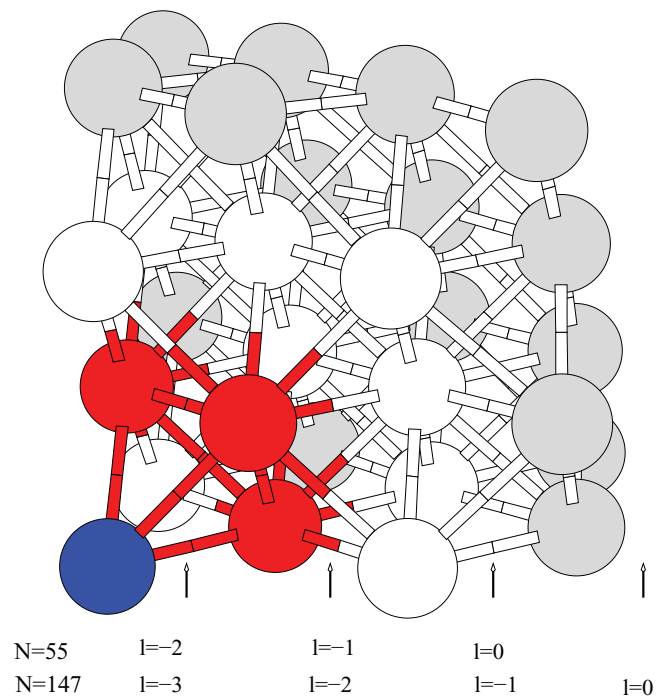


FIG. 1. (Color online) View of one-eighth of the cubo-octahedral cluster Pd_xPt_y ($x + y = 147$). The different colors correspond to the different cubo-octahedral layers within the cluster. The 55-atom cluster is formed with only the first three layers (blue, red, and white). The H atom will sit at different levels in interstitial positions between two layers or at the surface. The level $l = 0$ corresponds, for both sizes, to adsorption at the surface, whereas the most internal position of H corresponds to the level $l = -2$ for the 55-atom cluster and to the level $l = -3$ for the 147-atom cluster.

one expected led us to decrease the electronic temperature to 60 K. Despite this decrease the spectrum remained rather smooth, thus resembling the typical densities of states of bulk-like systems. Therefore, although this cluster size can still be considered in the range between the isolated atom and the bulk, it can be qualified as a bulk-like cluster in regard to its electronic spectrum. Thus, we believe that the 147-atom clusters retain the electronic trends of larger clusters experimentally characterized.^{13,18}

In the calculations, the clusters were placed in the center of a supercell with enough empty space to prevent interactions with their replica in adjacent cells. Only the Γ point was used when integrating over the Brillouin zone. Structural relaxation is performed with a conjugate gradient algorithm and is stopped when each force component at each atom is smaller than $0.01 \text{ eV}/\text{\AA}$. The interatomic distance found in the 147-atom Pd cluster (2.79 \AA) is very close to the calculated bulk value (2.83 \AA), which further supports the bulk-like character of these particles.

Finally, we performed careful tests for particular cases to ensure the quality and the stability of the obtained trends. The results were hardly modified when the double-zeta plus polarization basis was replaced by a triple- ζ single polarized basis³² as well as when using the DFT VASP code,^{33,34} against which we benchmarked also the results.

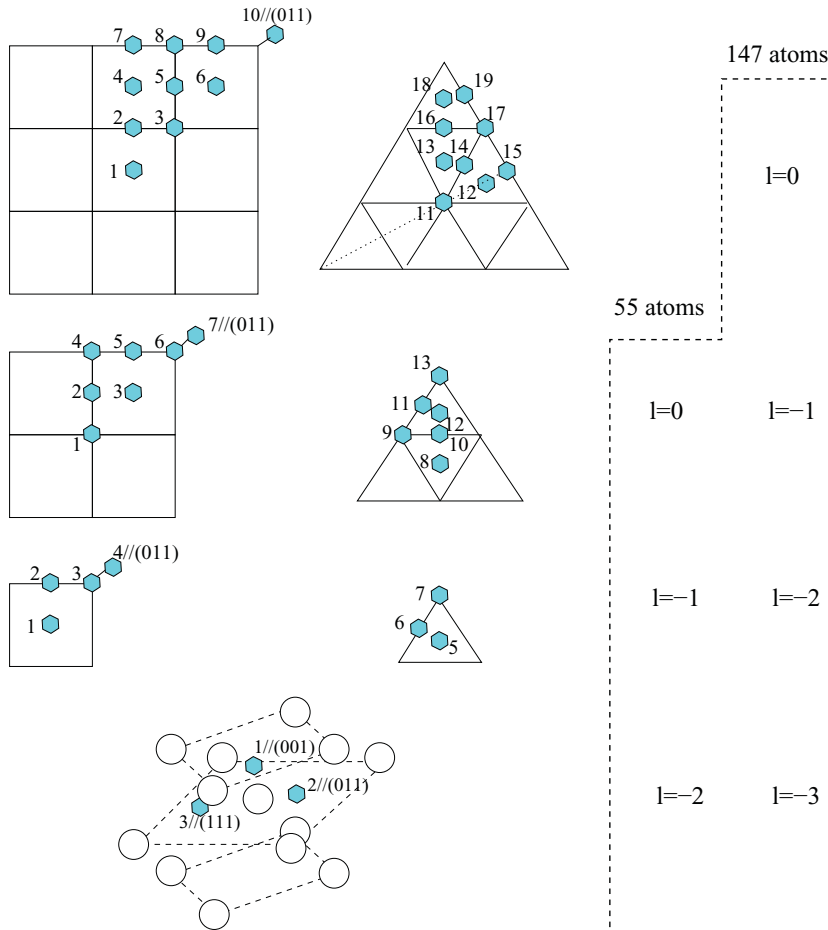


FIG. 2. (Color online) All the nonequivalent positions for the insertion of H (light blue hexagon) at the different interstitial levels within the cluster as well as at the surface. For the squared faces of the cluster, a shift along the (001) direction has to be considered, unless shown otherwise, since the plot only shows the projection. For the triangular faces, a shift along the (111) direction has to be considered.

III. RESULTS

In Fig. 1 we show one-eighth of the fcc cubo-octahedral structure of a 147-atom cluster. This cluster is formed with four concentric layers (including the central atom), with 1, 12, 42, and 92 atoms, respectively. These layers are illustrated with different colors in Fig. 1. In the 55-atom cubo-octahedral cluster Pd₁₃Pt₄₂, the Pt shell corresponds to the layer of 42 atoms surrounding a Pd core of 13 atoms. In the 147-atom

cubo-octahedral cluster Pd₁₃Pt₁₃₄, we have a Pt shell formed by the two external layers, while in Pd₅₅Pt₉₂, the Pt shell corresponds to the external layer of 92 atoms surrounding a Pd core of 55 atoms. Hydrogen is interstitially inserted in different positions between the different layers. (We also calculated the H adsorption at the surface positions.) In Fig. 1, the different levels between layers, at which H is interstitially inserted, are defined. The level $l = 0$ corresponds, in both cases, to

TABLE I. Characteristics of the stable positions for H inside or at the surface of the cubo-octahedral Pd₁₃Pt₄₂ cluster. The notation and type of the H sites, that is, the index and the level of the H position (according to Fig. 2) along with its geometrical environment, followed by the total energy difference (in meV) of H sitting in the different stable positions with respect to the most stable one, the chemical nature of the H neighbors, the volume (in Å³) available for H insertion (calculated in the H-unloaded clusters), and the volume change (in percentage) after H absorption. All the volumes are referred to a tetrahedral volume. Note that a pyramid contains two tetrahedrons, as indicated in parenthesis by the 2× symbol.

Stable H positions			Pd ₁₃ Pt ₄₂			
Index	Level	Environment	ΔE	H neighbors	Ω	ΔΩ/Ω
3	-2	tetrahedral	1234	4Pd	2.35	15.3
1	-1	pyramidal	767	4Pd-1Pt	2.65(2×)	13.6
1	0	top	381	1Pt		
2	0	bridge	0	2Pt		
5	0	bridge	155	2Pt		
7	0	top	406	1Pt		
8	0	hollow	530	3Pt		
12	0	hollow	390	3Pt		

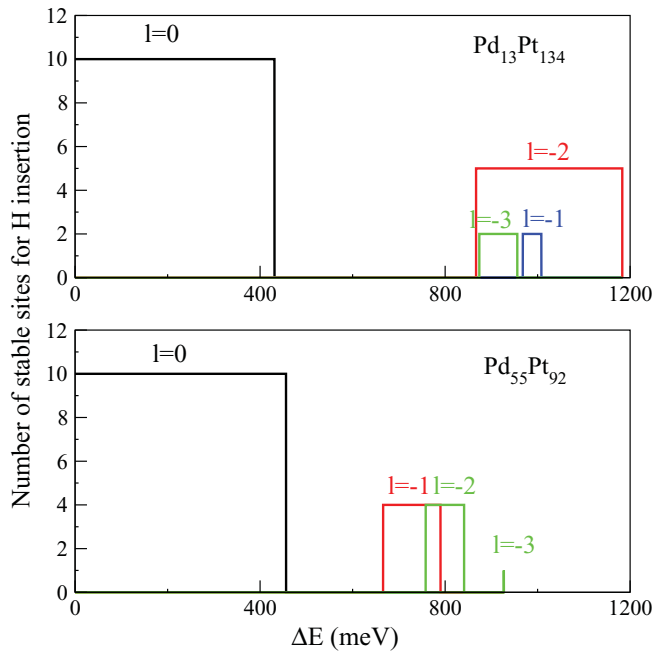


FIG. 3. (Color online) Spread in energy for H sitting at the different levels defined in Figs. 1 and 2, taking as a reference the energy of the most stable site. The black lines correspond to the surface sites (level $l = 0$), the red lines correspond to the interface level ($l = -2$ for $\text{Pd}_{13}\text{Pt}_{134}$ and $l = -1$ for $\text{Pd}_{55}\text{Pt}_{92}$), the green lines correspond to the internal sites inside the Pd core ($l = -3$ for $\text{Pd}_{13}\text{Pt}_{134}$ and $l = -2, -3$ for $\text{Pd}_{55}\text{Pt}_{92}$), and the blue line corresponds to the internal sites inside the Pt shell ($l = -1$ for $\text{Pd}_{13}\text{Pt}_{134}$). The height of each bar measures the number of stable sites found for H at the corresponding level.

adsorption at the surface. In Fig. 2 we illustrate, for both cluster sizes, the nonequivalent positions that H can occupy at each level within the system. We have explored all those possibilities. In what follows, we will identify each position of H by means of both the level l and the corresponding number according to Fig. 2.

Let us discuss first the results for H insertion in the 55-atom cluster $\text{Pd}_{13}\text{Pt}_{42}$. In Table I we report the total energy difference of H sitting in different positions with respect to the most stable one. Although we have tested all the nonequivalent positions illustrated in Fig. 2, we only found those reported in Table I since during the structural relaxation process some of the inputs converged to the same final site. In Table I we provide information about the local geometrical and chemical environment that the hydrogen atom finds in the different sites. The most stable positions of H are at the surface, particularly in bridge sites ($l = 0$, positions 2 and 5), followed by top and hollow sites. Inside the cluster, the most stable position for H is the pyramidal site at the interface ($l = -1$) in which H is surrounded by four Pd atoms and one Pt atom. The most internal position ($l = -2$) is a tetrahedral site, but it is far up in energy. Therefore, already for this cluster size, the interface is a favorable environment for H insertion, as observed for larger clusters through hydrogen-pressure measurements.¹³ Indeed, H atoms find larger volumes at the interface than in the Pd core. In the interface of $\text{Pd}_{13}\text{Pt}_{42}$, only one interstitial site (pyramidal) for H was energetically stable. The others did

not converge in the calculations. There is another possible interstitial site (a tetrahedral one corresponding to position 2 at $l = -1$ in Fig. 2) that was also tested as input. However, during the relaxation process the H atom moved away from this site toward the surface as if no effective barrier existed for it. In addition, for this cluster size, only one core/shell ratio can be taken with a minimum Pd core of 13 atoms.

In what follows we discuss the results for the larger clusters of 147 atoms, which are closer to the bulk-like limit and therefore to the experimental samples and in which different core/shell ratios can be explored, namely, $\text{Pd}_{13}\text{Pt}_{134}$ and $\text{Pd}_{55}\text{Pt}_{92}$. Again, all the different positions for H, according to Fig. 2, have been tested. As expected, for this cluster size we have found many more stable positions for H than in the smaller 55-atom cluster, particularly at the interface (level $l = -2$ for $\text{Pd}_{13}\text{Pt}_{134}$ and $l = -1$ for $\text{Pd}_{55}\text{Pt}_{92}$). In Fig. 3 we plot a diagram to show the spread in energy for H sitting at the different levels, taking as a reference the energy of the most stable site. In this diagram we notice that the level at which there are more available sites is $l = 0$, that is, the surface, which provides the most favorable positions of H in the absence of pressure; we also note that among the internal interstitial sites, those located at the interface are, overall, the most favorable ones ($l = -2$ for $\text{Pd}_{13}\text{Pt}_{134}$ and $l = -1$ for $\text{Pd}_{55}\text{Pt}_{92}$), in agreement with the experimental findings of Kobayashi *et al.*¹³ The interface of Pd and Pt, $l = -2$ in $\text{Pd}_{13}\text{Pt}_{134}$, provides the second largest number of stable positions. The thinness of the Pt shell of $\text{Pd}_{55}\text{Pt}_{92}$ is concomitant with a smaller energy separation between the internal sites and the surface sites as compared with $\text{Pd}_{13}\text{Pt}_{134}$.

In Table II we report the detailed data obtained for $\text{Pd}_{13}\text{Pt}_{134}$ and $\text{Pd}_{55}\text{Pt}_{92}$ from which Fig. 3 was built. As in the 55-atom clusters, the most favorable positions of H in the absence of pressure are at the surface, particularly in bridge positions, followed by top and hollow sites. On the surface of both clusters, hydrogen can sit in squared or triangular faces (see Fig. 2), with the squared face being the most favorable one. The large number of stable bridge sites offers many available sites for chemical reactions. The fact that the energy distribution is roughly the same for the two investigated systems suggests that the amount of Pt can be appreciably reduced in the catalysts. This is consistent with the reported results for M/Pt nanoparticles formed with an M core ($M = \text{Pd}, \text{Ir}, \text{Ru}$) surrounded by one or two Pt layers.^{18,19}

At the interface, the pyramidal position of H, for which H maximizes the number of Pd neighbors (four Pd neighbors and one Pt neighbor), is the most favorable site for both core/shell ratios. The next stable interfacial site for both core/shell ratios corresponds to a chemical environment where the number of Pd and Pt neighbors is equal (a tetrahedral site). Finally, in general, the richer the Pt environment is, the less stable the insertion site is. In the $\text{Pd}_{55}\text{Pt}_{92}$ cluster, we have not found stable interfacial sites for H with more than two Pt neighbors.

Within the pure Pd environment (inside the Pd core), H can also be stabilized in several sites. In $\text{Pd}_{13}\text{Pt}_{134}$, only two positions among the three possible ones in $l = -3$ are stable, the energy of which is comparable to that of the pyramidal sites at the interface. In $\text{Pd}_{55}\text{Pt}_{92}$, $l = -2$ and $l = -3$ correspond to the Pd core. In this case, the separation in energy between

TABLE II. Characteristics of the stable positions for H inside or at the surface of the two Pd core/Pt shell clusters of 147 atoms. The notation and type of the H sites, that is, the index and the level of the H position (see Fig. 2) as well as its geometrical environment are given first, followed by, for each clusters, the total energy difference (in meV) of H sitting in the different stable positions with respect to the most stable one, the chemical nature of the H neighbors, the volume (in \AA^3) available for H insertion in the H-free clusters, and the volume change in percentage after H absorption. all the volumes are referred to a tetrahedral volume. Note that a pyramid contains two tetrahedrons, as indicated in parenthesis by the $2\times$ symbol.

Stable H positions			$Pd_{13}Pt_{134}$				$Pd_{55}Pt_{92}$			
Index	Level	Environment	ΔE	H neighbors	Ω	$\Delta\Omega/\Omega$	ΔE	H neighbors	Ω	$\Delta\Omega/\Omega$
1	-3	pyramidal	874	5Pd	2.48(2 \times)	4.1				
3	-3	tetrahedral	956	4Pd	2.48	13.5	927	4Pd	2.45	14.2
1	-2	pyramidal	867	4Pd-1Pt	2.59(2 \times)	4.4	758	5Pd	2.54(2 \times)	4.4
2	-2	tetrahedral	1064	2Pd-2Pt	2.57	14.6	833	4Pd	2.49	13.7
3	-2	pyramidal	1163	1Pd-4Pt	2.52(2 \times)	6.7				
5	-2	octahedral	1088	3Pd-3Pt	2.62(4 \times)	2.1	759	6Pd	2.50(4 \times)	3.6
7	-2	tetrahedral	1183	1Pd-3Pt	2.52	16.9	841	4Pd	2.46	13.8
2	-1	tetrahedral					790	2Pd-2Pt	2.58	18.4
3	-1	pyramidal	968	5Pt	2.65(2 \times)	17.2	666	4Pd-1Pt	2.61(2 \times)	9.6
5	-1	tetrahedral					717	2Pd-2Pt	2.61	17.3
8	-1	tetrahedral	1008	4Pt	2.76	19.5	771	3Pd-1Pt	2.66	14.0
1	0	hollow					353	4Pt		
2	0	bridge	101	2Pt			67	2Pt		
3	0	top	339	1Pt			342	1Pt		
5	0	bridge	145	2Pt			129	2Pt		
7	0	bridge	0	2Pt			0	2Pt		
9	0	bridge	192	2Pt			208	2Pt		
10	0	top	354	1Pt			353	1Pt		
11	0	top	431	1Pt			465	1Pt		
13	0	hollow	407	3Pt			456	3Pt		
17	0	top	306	1Pt						
18	0	hollow	387	3Pt			426	3Pt		

the internal sites and the interfacial ones is larger than for $Pd_{13}Pt_{134}$. We note that the smaller Pt/Pd atomic ratio of $Pd_{55}Pt_{92}$ is closer to the experimental samples. Finally, the H atom can sit in an internal pure Pt environment (inside the Pt shell) only for $Pd_{13}Pt_{134}$ ($l = -1$). No such environment exists in $Pd_{55}Pt_{92}$ because it has a Pt shell formed with a single cubo-octahedral layer.

In order to better understand why the interface provides so favorable an environment for metal-hydride formation inside these core/shell clusters, it is pertinent to analyze the change in the atomic arrangements upon H insertion. As in the case of Fe/V multilayers⁵⁻⁹ and the Mg/Ti ones investigated by Baldi *et al.*,¹² structural distortions can also play an important role in the hydrogen absorption properties. We have calculated the available volume for H insertion Ω in the different internal sites as well as the volume change upon H insertion $\Delta\Omega/\Omega$. The H atom can stand in tetrahedral, pyramidal, or octahedral environments. A pyramid is made of two tetrahedrons, and an octahedron contains four tetrahedrons. All the volumes are thus referred to a tetrahedral volume, and for instance, the volume of a pyramid is obtained as the sum of the volume of two tetrahedrons. The volume of a tetrahedron is easily derived from the length of its edges, according to the Cayley-Menger determinant.³⁵ The corresponding values are reported in Table II for $Pd_{13}Pt_{134}$ and $Pd_{55}Pt_{92}$. We note that in both cases, the smaller available volume corresponds to sites inside the Pd core, a fact that does not favor the H

absorption at these sites. In this respect, interfacial sites and sites inside the Pt shell are more favorable as they provide a larger available volume. However, the lattice distortion upon H loading and the concomitant energy cost also play an important role. The volume change upon H absorption is, in general, larger when H is absorbed inside the Pt shell than when it sits at the interface or inside the Pd core. This trend does not favor the H absorption inside the Pt shell. Overall, the best compromise between both trends is achieved mainly at the interface, which could explain why it offers a favorable environment for metal-hydride formation. It is worth noting that the atomic environments less affected by H insertion contain a squared face, that is, a pyramidal or an octahedral environment. As a general trend, overall, the most stable insertion sites are pyramidal interstices offering a volume for H comprised around $2 \times 2.60 \text{ \AA}^3$, with a moderate atomic rearrangement upon H insertion and in which the H atom maximizes the number of Pd neighbors. According to our theoretical predictions, a suitable local environment for H loading is the one having Pd and Pt with a larger amount of Pd atoms. On the one hand, Pt atoms have a trend to expand the available volume. On the other hand, the richer Pd environment ensures a moderate volume expansion upon H loading with a moderate insertion energy cost. In fact, Pd has smaller shear modulus than Pt, and as reported by Meded and Mirbt,¹¹ this favors the reduction of the elastic energy upon H storage. Hence, if these arguments based on

the local environment were extrapolated from the core/shell configuration to a homogeneous alloy configuration, alloying of these bimetallic clusters with a weak proportion of Pt should be very favorable for H insertion, as demonstrated through coupled hydrogen pressure-composition and NMR measurements by Kobayashi *et al.*¹⁴ In the present system the enhancement of the absorption capacity is obtained by the association of two elements, i.e., Pd and Pt, which present a substantial contrast in shear moduli.

IV. CONCLUSIONS

In summary, we have investigated, using the density functional theory, the absorption and adsorption of hydrogen in all the nonequivalent positions available inside and at the surface of the Pd core/Pt shell cubo-octahedral NPs Pd₁₃Pt₄₂, Pd₁₃Pt₁₃₄, and Pd₅₅Pt₉₂. The most favorable positions for H in the absence of pressure are found when it is adsorbed at the surface, specifically on bridge sites. The Pt content could be decreased since it is demonstrated that the energy distribution is roughly the same for the two investigated systems. Among the internal sites, the interface is, overall, the most favorable environment for metal-hydride formation, in agreement with recent hydrogen pressure-composition and NMR measurements of Kobayashi *et al.*¹³ The atomic environments less affected by H loading and most favorable for its loading contain a squared face. The Pd core provides the smaller available volume for H insertion, while the larger local atomic rearrangement upon H insertion takes place in the Pt shell. As

a general trend, the most stable absorption sites are pyramidal interstices at the interface offering a volume for H of around $2 \times 2.60 \text{ \AA}^3$, with a moderate atomic rearrangement upon H insertion and in which the H atom maximizes the number of Pd neighbors. Interfacial effects like roughness are likely to occur under certain experimental conditions. Considering the fact that H insertion strongly depends on the local environment and provided that a mixed Pd-Pt environment favors H insertion, we expect that roughness will favor a wider region for H insertion at the interface. Roughness implies intermixing of Pd and Pt; the most extreme case of intermixing is the formation of the homogeneous alloy. Work is currently in progress for Pd/Pt clusters with arrangements other than the ideal Pd core/Pt shell in the context of hydrogen insertion.

ACKNOWLEDGMENTS

We acknowledge the financial support from the Spanish Ministry of Science and Innovation in conjunction with the European Regional Development Fund (Project FIS2008-02490/FIS) and the Junta de Castilla y León. We also acknowledge the numerical support of the Pole de Calcul Intensif pour la Mer in Brest. A.V. acknowledges the financial support and the kind hospitality from the Université de Brest (UBO), France. F.A.G. acknowledges the financial support from PROMEP-SEP-CA230, CONACyT (México) Grant No. 2005-50650. A.G.F. thanks the Spanish Ministry of Science and Innovation for a FPU Grant.

¹P. Vajeeston, P. Ravindran, and H. Fjellvag, *J. Alloys Compd.* **446-447**, 44 (2007).

²Y. Filinchuk, D. Chernyshov, A. Nevidomskyy, and V. Dmitriev, *Angew. Chem., Int. Ed.* **47**, 529 (2008).

³Y. Filinchuk, R. Czerny, and H. Hagemann, *Chem. Mater.* **21**, 925 (2009).

⁴H. Arashima, F. Takahashi, T. Ebisawa, H. Itoh, and T. Kabutomori, *J. Alloys Compd.* **356-357**, 405 (2003).

⁵S. Ostanin, V. M. Uzdin, C. Demangeat, J. M. Wills, M. Alouani, and H. Dreyssé, *Phys. Rev. B* **61**, 4870 (2000).

⁶V. Leiner, K. Westerholt, A. M. Blixt, H. Zabel, and B. Hjörvarsson, *Phys. Rev. Lett.* **91**, 037202 (2003).

⁷D. Labergerie, K. Westerholt, H. Zabel, and B. Hjörvarsson, *J. Magn. Magn. Mater.* **225**, 373 (2001).

⁸A. Remhof, G. Nowak, A. Nefedov, H. Zabel, M. Björck, M. Pärnaste, and B. Hjörvarsson, *Superlattices Microstruct.* **41**, 127 (2007).

⁹G. Andersson, B. Hjörvarsson, and H. Zabel, *Phys. Rev. B* **55**, 15905 (1997).

¹⁰T. Dziekan, V. Meded, S. Mirbt, S. Shallcross, B. Hjörvarsson, and P. Zahn, *Phys. Rev. B* **79**, 012402 (2009).

¹¹V. Meded and S. Mirbt, *Phys. Rev. B* **71**, 024207 (2005).

¹²A. Baldi, G. K. Pálsson, M. Gonzalez-Silveira, H. Schreuders, M. Slaman, J. H. Rector, G. Krishnan, B. J. Kooi, G. S. Walker, M. W. Fay, B. Hjörvarsson, R. J. Wijngaarden, B. Dam, and R. Griessen, *Phys. Rev. B* **81**, 224203 (2010).

¹³H. Kobayashi, M. Yamauchi, H. Kitagawa, Y. Kubota, K. Kato, and M. Takata, *J. Am. Chem. Soc.* **130**, 1818 (2008).

¹⁴H. Kobayashi, M. Yamauchi, H. Kitagawa, Y. Kubota, K. Kato, and M. Takata, *J. Am. Chem. Soc.* **132**, 5576 (2010).

¹⁵M. Yamauchi and H. Kitagawa, *Synth. Met.* **153**, 353 (2005).

¹⁶C. Sachs, A. Pundt, R. Kirchheim, M. Winter, M. T. Reetz, and D. Fritsch, *Phys. Rev. B* **64**, 075408 (2001).

¹⁷Y. Isobe, M. Yamauchi, R. Ikeda, and H. Kitagawa, *Synth. Met.* **135**, 757 (2003).

¹⁸A. U. Nilekar, S. Alayoglu, B. Eichhom, and M. Mavrikakis, *J. Am. Chem. Soc.* **132**, 7418 (2010).

¹⁹V. Mazumder, M. Chi, K. L. More, and S. Sun, *J. Am. Chem. Soc.* **132**, 7848 (2010).

²⁰B. Coq and F. Figueras, *J. Mol. Catal. A* **173**, 117 (2001).

²¹L. O. Paz-Borbón, R. L. Johnston, G. Barcaro, and A. Fortunelli, *J. Phys. Chem. C* **111**, 2936 (2007).

²²D. J. Borbón-González, R. Pacheco-Contreras, A. Posada Amarillas, J. C. Schön, R. L. Johnston, and J. M. Montejano-Carrizales, *J. Phys. Chem. C* **113**, 15904 (2009).

²³R. Pacheco-Contreras, A. Arteaga-Guerrero, D. J. Borbón-González, A. Posada Amarillas, J. C. Schön, and R. L. Johnston, *J. Comput. Theor. Nanosci.* **7**, 199 (2010).

²⁴J. M. Soler, E. Artacho, J. D. Gale, A. García, J. Junquera, P. Ordejon, and D. Sánchez-Portal, *J. Phys. Condens. Matter* **14**, 2745 (2002).

²⁵P. Ordejon, E. Artacho, and J. M. Soler, *Phys. Rev. B* **53**, R10441 (1996).

- ²⁶D. Sanchez-Portal, P. Ordejon, E. Artacho, and J. M. Soler, *Int. J. Quantum. Chem* **65**, 453 (1997).
- ²⁷J. P. Perdew, K. Burke, and M. Ernzerhof, *Phys. Rev. Lett.* **77**, 3865 (1996).
- ²⁸N. Troullier and J. L. Martins, *Phys. Rev. B* **43**, 1993 (1991).
- ²⁹L. Kleinman and D. M. Bylander, *Phys. Rev. Lett.* **48**, 1425 (1982).
- ³⁰F. Aguilera-Granja, R. C. Longo, L. J. Gallego, and A. Vega, *J. Chem. Phys.* **132**, 184507 (2010).
- ³¹S. G. Louie, S. Froyen, and M. L. Cohen, *Phys. Rev. B* **26**, 1738 (1982).
- ³²J. Junquera, Ó. Paz, D. Sánchez-Portal, and E. Artacho, *Phys. Rev. B* **64**, 235111 (2001).
- ³³G. Kresse and J. Hafner, *Phys. Rev. B* **47**, 558 (1993).
- ³⁴G. Kresse and J. Furthmüller, *Phys. Rev. B* **54**, 11169 (1996).
- ³⁵D. M. Y Sommerville, *An Introduction to the Geometry of n Dimensions* (Dover, New York, 1958), p. 124.